NASA TECHNICAL NOTE

EXPERIMENTAL STAGNATION-POINT VELOCITY GRADIENTS AND HEAT-TRANSFER COEFFICIENTS FOR A FAMILY OF BLUNT BODIES AT MACH 8 AND ANGLES OF ATTACK

by James C. Ellison

Langley Research Center
Langley Station, Hampton, Va.

NATIONAL AERONAUTICS AND SPACE ADMINISTRATION • WASHINGTON, D. C. • APRIL 1969

EXPERIMENTAL STAGNATION-POINT VELOCITY GRADIENTS AND HEAT-TRANSFER COEFFICIENTS FOR A FAMILY OF BLUNT BODIES AT MACH 8 AND ANGLES OF ATTACK

By James C. Ellison

Langley Research Center
Langley Station, Hampton, Va.

NATIONAL AERONAUTICS AND SPACE ADMINISTRATION

For sale by the Clearinghouse for Federal Scientific and Technical Information
Springfield, Virginia 22151 – CFSTI price $3.00

EXPERIMENTAL STAGNATION-POINT VELOCITY GRADIENTS AND HEAT-TRANSFER COEFFICIENTS FOR A FAMILY OF BLUNT BODIES AT MACH 8 AND ANGLES OF ATTACK*

By James C. Ellison
Langley Research Center

SUMMARY

Local pressure and heat-transfer measurements have been obtained on a family of blunt, axisymmetric bodies having a range of ratios of body radius to nose radius from 0 (flat face) to 0.707, and ratios of corner radius to body radius of 0 (sharp corner) to 0.40. The experimental data were obtained at a Mach number of 8.0 and a Reynolds number (based on model diameter) of 1.37×10^6, over a range of angles of attack from 0^o to 20^o.

Determination of the stagnation-point location indicated that at angles of attack the stagnation point does not occur at the most forward point on the body, and the variation of stagnation-point location with angle of attack is approximately linear for all bodies investigated.

An effective nose radius has been determined for each body at several angles of attack. This effective nose radius can be employed to calculate the stagnation-point values of the heat-transfer coefficient. The results indicate that the stagnation-point heat-transfer coefficient for a given body geometry varies about 10 percent with angle of attack, except for the flat-faced body having the largest corner radius.

INTRODUCTION

Blunt-faced reentry configurations and blunt bodies of revolution have been extensively investigated at zero angle of attack to determine the effects of body shape variables on the flow parameters (refs. 1 to 9). However, results at angles of attack have been restricted to specific configurations such as Gemini and Apollo (refs. 10 and 11).

*The information presented herein is based in part upon a thesis entitled "The Effects of Nose and Corner Radii on the Flow About Blunt Bodies at Angle of Attack" submitted in partial fulfillment of the requirements for the degree of Master of Science in Aerospace Engineering, Virginia Polytechnic Institute, Blacksburg, Virginia, August 1967.

To obtain a more complete understanding of flow about blunt bodies at angles of attack, the effects of nose and corner radii on the surface pressure distribution, stagnation-point velocity gradient and heat-transfer coefficient, shock standoff distance, and stagnation-point location have been obtained at a Mach number of 8. The results of this investigation are presented herein and are compared with previous data and the results of several theoretical methods.

An effective nose radius which was employed successfully to correlate data for effects of variable model geometry at zero angle of attack in references 1 and 6 has been extended to angles of attack in this investigation.

SYMBOLS

c_p	specific heat at constant pressure
H	total enthalpy
h	heat-transfer coefficient
h_{ref}	reference heat-transfer coefficient, 0.01 Btu/ft^2-sec-$^\circ$R (204 watts/meter^2-$^\circ$K)
K	bluntness parameter, R_B/R_N
p	local surface pressure
p_t	local surface pressure at stagnation point
Q	correction factor between three-dimensional and axisymmetric flow, ≤ 1
R	ratio of corner radius to body radius, R_c/R_B
R_B	body radius
R_c	corner radius
R_{eff}	effective nose radius
R_N	nose radius

r	radial coordinate
r_b	model base radius
s	distance along surface, measured from stagnation point
s_o	distance along surface, measured from center of face
s_1	distance along surface from center of face to the point where the nose and corner radii are tangent
T	temperature
T_t	total temperature
T_w	wall temperature
t	time
U	resultant velocity gradient, $\left[\left(U_s^2 + U_y^2\right)/2\right]^{1/2}$
U_s	stagnation-point velocity gradient along surface in s-direction (fig. 1)
U_{sp}	spherical stagnation-point velocity gradient
U_y	stagnation-point velocity gradient along surface perpendicular to the s-direction (fig. 1)
u	velocity component
α	angle of attack
γ	ratio of specific heats
Δ	stagnation-point shock detachment distance
ρ	density
τ	skin thickness

ϕ angle between the axis of symmetry and a vector normal to the surface at the stagnation point

Subscripts:

calc calculated value based on effective nose radius

meas measured value

Measurements for this investigation were taken in the U.S. Customary System of Units. Equivalent values are indicated parenthetically in the International System of Units (SI). Details concerning the use of SI, together with physical constants and conversion factors, are given in reference 12.

APPARATUS AND TEST PROCEDURE

The experimental phase of this investigation was conducted in the Langley Mach 8 variable-density tunnel, which is an intermittent blowdown tunnel equipped with a quick-injection mechanism and schlieren system. Basically, the tunnel consists of a heat exchanger, a contoured axisymmetric nozzle, an 18-inch-diameter (45.7 cm) test section, a diffuser, and a vacuum system.

The pressure and heat-transfer tests were conducted in air at an average stagnation temperature of 1460° R (811° K) and average stagnation pressure of 1000 psia (6895 kN/m^2). The corresponding free-stream Mach number and Reynolds number (based on model diameter) were 8.0 and 1.37×10^6, respectively. Run times of about 90 seconds were necessary for the pressure tests, but the heat-transfer tests required only about 5 seconds of run time. Data were obtained for angle of attack from 0° to 20°.

The model geometry is shown in figure 1 with a sketch of each model and its dimensions. A total of 18 models, representing nine bodies, were tested. All models had a radius R_B of 2.0 inches (5.08 cm).

Each pressure model was constructed from type 347 stainless steel and had a 0.100-inch (0.254-cm) skin. Pressure orifices were formed by the inside diameter (0.040-inch (0.102-cm)) of a stainless-steel tube. A row of orifices was located on the face of the model in a vertical plane of symmetry. The orifices were spaced approximately 0.150 inch (0.381 cm) apart, measured along the surface. Additional rows of orifices were placed normal to the primary row across the face of the model.

The heat-transfer models were constructed from 17-4 PH stainless steel and had a 0.030-inch (0.076-cm) skin. Thermocouple wires were welded to the inside of the skin

and were arranged in the same manner as the pressure orifices, but they were spaced at 0.100-inch (0.254-cm) intervals. The skin-thickness at each thermocouple location is believed to be accurate within ±5 percent.

In the pressure tests, the angle of attack was varied to obtain a stagnation point on the orifice at each intersection of the primary row and the normal rows. In addition, the position of the model in the tunnel and the angle of attack were measured; and the corresponding heat-transfer models were tested in the same position.

A dial gage and a precision barometer were used to determine the stagnation pressure. The local pressures on the bodies were calculated from measurements of fluid levels on manometer boards and were nondimensionalized by the measured pressure at the stagnation point. The pressures near the stagnation point were measured on butyl phthalate manometers, and the remaining pressures were measured on mercury manometers.

Heat-transfer data were obtained by using a transient testing technique, and the millivolt output of the thermocouples was read from magnetic tapes and converted to temperatures on a digital computer. The stagnation-point heat-transfer coefficients were obtained by fitting a second-degree curve to the temperature-time data by the method of least squares. The time derivative of temperature was computed from the fitted curve on a card-programed computer, and the heat-transfer coefficient was determined from the expression

$$h = \frac{\rho c_p \tau}{T_t - T_w} \frac{dT}{dt} \tag{1}$$

Schlieren photographs were taken during each test run, and the stagnation-point shock standoff distance was determined from these photographs.

RESULTS AND DISCUSSION

The measured and computed results obtained in this investigation are presented in figures 2 to 9, and the pertinent parameters are summarized in table I.

Zero-Angle-of-Attack Data

Presented in figure 2 are the pressure distributions at zero angle of attack for the nine bodies investigated. The ratio of the local pressure to the stagnation-point pressure is shown as a function of the surface distance divided by the body radius. The data for the three sharp-cornered bodies are compared with several theories in figure 3.

With these pressure distributions, the velocity distributions were calculated by assuming an isentropic expansion along the body from the stagnation point and using the expression

$$\frac{u}{\sqrt{2H}} = \left[1 - \left(\frac{p}{p_t}\right)^{\frac{\gamma-1}{\gamma}}\right]^{1/2} \tag{2}$$

to determine the velocity. The stagnation-point velocity gradients were determined by plotting the velocity distribution and taking the slope of the straight line through the data on either side of the stagnation point. In figures 4(a) and 4(b), R_B/R_{eff} is shown as a function of the parameters K and R. These results were obtained from the relation $R_B/R_{eff} = U/U_{sp}$, presented by Zoby and Sullivan in reference 6. The stagnation-point velocity gradient U_{sp} was calculated from Newtonian theory for a sphere having a radius equal to the radius R_B of the bodies investigated. Newtonian theory and the results of reference 6 are also shown in figure 4(a). It is seen that the effective nose radius R_{eff} decreases as the nose radius decreases (fig. 4(a)) and as the corner radius increases (fig. 4(b)). The data of the present investigation agree with the results of Zoby and Sullivan (ref. 6) within 10 percent for $K = 0$ and $K = 0.707$; however, for $K = 0.417$ and $R = 0$, the disagreement is about 20 percent.

Angle-of-Attack Data

The pressure distributions for each body at several angles of attack are shown in figure 5. The stagnation-point locations as a function of angle of attack were determined for each body, and are presented in figure 6. The data indicate that the variation in stagnation-point location with angle of attack is approximately linear, and the stagnation point does not occur at the most forward point on the body at angles of attack.

The parameter R_B/R_{eff} is presented as a function of angle of attack for the various combinations of nose and corner radii in figure 7, and was determined in the same manner as for $\alpha = 0$. The parameter R_{eff} was taken to be the radius of a sphere which, according to Newtonian theory, would have a velocity gradient equal to $\left[\left(U_s^2 + U_y^2\right)/2\right]^{1/2}$ The change in R_B/R_{eff} with angle of attack is less than 10 percent at angles of attack less than 12^o except for the flat-faced body with the large corner radius. In general, the parameter R_B/R_{eff} decreases as angle of attack increases up to about 10^o, and then begins increasing with angle of attack.

Heat-transfer results for the models at angles of attack are shown in figure 8. The data are presented as the ratio of the measured stagnation-point heat-transfer coefficient to the heat-transfer coefficient calculated for a sphere (having the effective nose radius obtained from the present investigation). A Prandtl number of 0.72 was used to calculate

the values of h_{calc} by the theory of Reshotko and Cohen (ref. 4). The results for the bodies having $K = 0.707$ and 0.417 show good agreement with the calculated data. (Data for the sharp-cornered body with $K = 0.707$ were not obtained at angles of attack because of a malfunction in the thermocouples on this model.) While this technique tends to underpredict the values on the flat-faced bodies, the data are in agreement with the data of Jones (ref. 10), and therefore the values obtained for the effective nose radius on these bodies are believed to be valid.

Listed in table I are the data employed to obtain the results presented in figures 8 and 9, as well as the theoretical correction factors obtained by Libby (ref. 13), by Reshotko (ref. 14), and in the present investigation. To use the methods of references 13 and 14, the principal velocity gradient U_S and the normal velocity gradient U_y at the stagnation point must be known. A value for the heat-transfer rate is calculated on the basis of the principal velocity gradient, assuming axisymmetric flow, and is multiplied by the correction factor to obtain the actual heat-transfer rate.

The present technique for determining the heat-transfer coefficient (or other parameters) requires only an effective nose radius for a given body. The heat transfer is taken to be that of a sphere having a radius equal to the effective nose radius of the body. (See table I for the heat-transfer coefficients calculated by this method and the experimentally obtained heat-transfer coefficients.)

The accuracy of the effective nose radius for predicting the stagnation-point heat-transfer coefficient has been evaluated by comparing the results of the present investigation with the results of Libby and Reshotko (refs. 13 and 14, respectively). This was accomplished by determining the correction factor Q, which is the ratio of the theoretical three-dimensional stagnation-point heat-transfer coefficient to the theoretical axisymmetric stagnation-point heat-transfer coefficient based on the maximum velocity gradient at the stagnation point. A close evaluation of the method for predicting the heat-transfer coefficient based on R_{eff} indicates excellent agreement with the methods of references 13 and 14. The trend of the measured heat-transfer $\left(h_{meas}/h_{ref}\right)$ data is not always in agreement with the theoretical predictions $\left(h_{calc}/h_{ref}\right)$. For instance, the calculated values indicate that for $\alpha = 0$ the stagnation-point heat-transfer coefficient increases as the corner radius increases for a given nose radius; however, the experimental data do not consistently show the same trend. This inconsistency is attributed to possible errors of ± 10 percent in the heat-transfer data due to inability to measure the skin thickness exactly.

In figure 9 the ratio of the measured shock detachment distance to the effective nose radius is shown as a function of angle of attack. Results presented by Van Dyke and Gordon (ref. 15) indicate that at a Mach number of 8 the value of Δ/R_B is 0.14 for a sphere. The results shown in figure 9 indicate that the effect of geometry and angle of

attack on shock detachment distance cannot, in general, be correlated very well by the effective nose radius. Presented in figure 5 of reference 16 are some results obtained at a Mach number of 10.5 on a flat-faced cylinder with rounded shoulders. Although these data are not shown in figure 9, they agree with the results in table I for similar bodies.

CONCLUDING REMARKS

Local pressure distributions, stagnation-point heat-transfer coefficients, and shock detachment distances were determined for a family of blunt bodies at angles of attack up to 20°. The data were obtained at a free-stream Mach number of 8.0 and Reynolds number of 1.37×10^6.

Determination of the stagnation-point location indicated that at angles of attack the stagnation point does not occur at the most forward point on the body, and the variation of stagnation-point location with angle of attack is approximately linear for all bodies investigated.

An effective nose radius has been determined for each body at several angles of attack. This effective nose radius can be employed to calculate the stagnation-point values of the heat-transfer coefficient. The results indicate that the stagnation-point heat-transfer coefficient for a given body geometry varies about 10 percent with angle of attack, except for the flat-faced body having the largest corner radius. Also, the stagnation-point heat-transfer coefficient based on the effective nose radius is shown to be in good agreement with the theoretical results of Libby and Reshotko.

Langley Research Center,
National Aeronautics and Space Administration,
Langley Station, Hampton, Va., January 30, 1969,
129-01-03-07-23.

REFERENCES

1. Boison, J. Christopher; and Curtiss, Howard A.: An Experimental Investigation of Blunt Body Stagnation Point Velocity Gradient. ARS J., vol. 29, no. 2, Feb. 1958, pp. 130-135.

2. Griffith, B. J.; and Lewis, Clark H.: A Study of Laminar Heat Transfer to Spherically Blunted Cones and Hemisphere-Cylinders at Hypersonic Conditions. AEDC-TDR-63-102 (Contract No. AF 40(600-1000), Arnold Eng. Dev. Center, June 1963.

3. Cleary, Joseph W.: An Experimental and Theoretical Investigation of the Pressure Distribution and Flow Fields of Blunted Cones at Hypersonic Mach Numbers. NASA TN D-2969, 1965.

4. Reshotko, Eli; and Cohen, Clarence B.: Heat Transfer at the Forward Stagnation Point of Blunt Bodies. NACA TN 3513, 1955.

5. Cooper, Morton; and Mayo, Edward E.: Measurements of Local Heat Transfer and Pressure on Six 2-Inch-Diameter Blunt Bodies at a Mach Number of 4.95 and at Reynolds Numbers Per Foot up to 81×10^6. NASA MEMO 1-3-59L, 1959.

6. Zoby, Ernest V.; and Sullivan, Edward M.: Effects of Corner Radius on Stagnation-Point Velocity Gradients on Blunt Axisymmetric Bodies. NASA TM X-1067, 1965.

7. Truitt, Robert Wesley: Hypersonic Aerodynamics. The Ronald Press Co., c.1959.

8. Li, Ting-Yi; and Geiger, Richard E.: Stagnation Point of a Blunt Body in Hyperonsic Flow. J. Aeron. Sci., vol. 24, no. 1, Jan. 1957, pp. 25-32.

9. Probstein, Ronald F.: Inviscid Flow in the Stagnation Point Region of Very Blunt-Nosed Bodies at Hypersonic Flight Speeds. WADC TN 56-395 (Contract No. AF 33(616)-2798), U.S. Air Force, Sept. 1956. (Available from DDC as AD97273.)

10. Jones, Robert A.: Heat-Transfer and Pressure Distributions on a Flat-Face Rounded-Corner Body of Revolution With and Without a Flap at a Mach Number of 8. NASA TM X-703, 1962.

11. Seidman, Mitchell: Heat Transfer and Pressure Distribution on a Two-Dimensional Blunted Asymmetric Body. Tech. Rep. 204 (Contract AF 33(616)-6692), Gen. Appl. Sci. Lab., Inc., Dec. 1960. (Available from DDC as AD 256 185.)

12. Mechtly, E. A.: The International System of Units – Physical Constants and Conversion Factors. NASA SP-7012, 1964.

13. Libby, Paul A.: Heat and Mass Transfer at a General Three-Dimensional Stagnation Point. NASA CR-817, 1967.

14. Reshotko, Eli: Heat Transfer to a General Three-Dimensional Stagnation Point. Jet Propulsion, vol. 28, Jan. 1958, pp. 58-60.

15. Van Dyke, Milton D.; and Gordon, Helen D.: Supersonic Flow Past a Family of Blunt Axisymmetric Bodies. NASA TR R-1, 1959.

16. Inouye, Mamoru; Marvin, Joseph G.; and Sinclair, A. Richard: Comparison of Experimental and Theoretical Shock Shapes and Pressure Distributions on Flat-Faced Cylinders at Mach 10.5. NASA TN D-4397, 1968.

TABLE I.- VALUES OF MEASURED AND CALCULATED PARAMETERS

K	R	α, deg	U_s	U_y	U	$\frac{R_B}{R_{eff}}$	$\frac{\Delta}{R_B}$	$\frac{h_{meas}}{h_{ref}}$	$\frac{h_{calc}}{h_{ref}}$	Q from – Libby (ref. 13)	Q from – Reshotko (ref. 14)	Q from – Present investigation
0.707	0	0	0.392	0.392	0.392	0.738	0.194	1.898	1.752	1.000	1.000	1.000
		8	.374	.397	.385	.726	.201	-----	1.780	.984	.988	.985
		16.25	.348	.372	.360	.678	.194	-----	1.724	.982	.985	.984
.707	.2	0	.410	.410	.410	.772	.196	1.815	1.828	1.000	1.000	1.000
		8	.360	.408	.385	.724	.200	1.776	1.750	.969	.974	.971
		19	.424	.418	.419	.788	.192	1.952	1.836	.997	.996	.993
.707	.4	0	.434	.434	.434	.817	.192	1.714	1.954	1.000	1.000	1.000
		10	.424	.420	.422	.795	.192	1.702	1.914	.998	.998	.997
		20	.363	.416	.390	.733	.178	1.668	1.839	.965	.972	.969
.417	0	0	.312	.312	.312	.587	.298	1.649	1.604	1.000	1.000	1.000
		6	.302	.264	.284	.534	.302	1.596	1.497	.966	.972	.969
		15.5	.298	.262	.281	.529	.263	1.647	1.490	.968	.974	.971
.417	.2	0	.323	.323	.323	.609	.287	1.577	1.645	1.000	1.000	1.000
		5.5	.281	.296	.288	.543	.283	1.609	1.512	.987	.989	.987
		13.75	.328	.303	.316	.595	.258	1.636	1.579	.979	.983	.981
.417	.4	0	.340	.340	.340	.640	.272	1.663	1.712	1.000	1.000	1.000
		9	.330	.333	.332	.624	.255	1.604	1.691	.998	.998	.998
		16	.419	.274	.354	.667	.221	1.672	1.755	.905	.924	.920
0	0	0	.168	.168	.168	.317	.491	1.448	1.208	1.000	1.000	1.000
		5	.162	.176	.169	.318	.500	1.441	1.195	.978	.982	.980
		12	.170	.160	.165	.310	.441	1.511	1.176	.983	.988	.985
		14.5	.238	.197	.219	.411	.387	1.448	1.300	.951	.962	.959
0	.2	0	.200	.200	.200	.377	.421	1.569	1.293	1.000	1.000	1.000
		5.5	.178	.196	.187	.353	.391	1.561	1.253	.975	.979	.978
		12.5	.263	.203	.235	.442	.325	1.597	1.408	.938	.955	.945
		18.5	.500	.247	.395	.743	.233	1.903	1.841	.860	.888	.888
0	.4	0	.242	.242	.242	.455	.349	1.406	1.453	1.000	1.000	1.000
		7.5	.186	.194	.190	.358	.340	1.457	1.282	.988	.990	.991
		11.75	.291	.304	.298	.561	.268	1.967	1.601	.986	.990	.989
		19.0	.308	.386	.349	.658	.161	1.962	1.730	.945	.955	.951

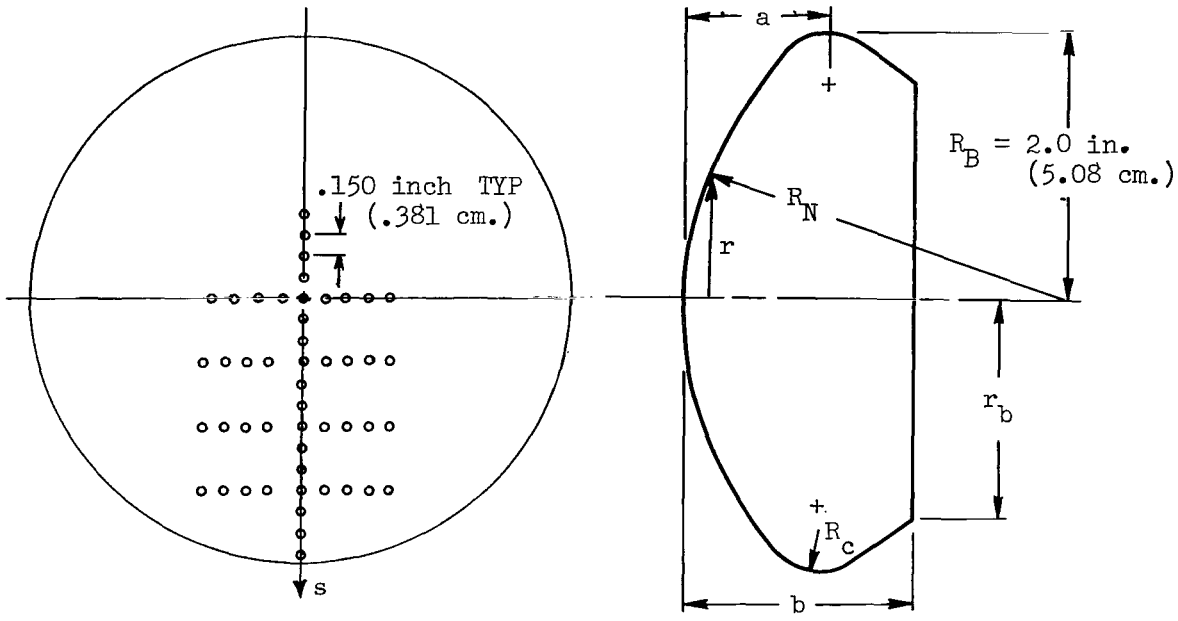

Model Shape	Model	K	R	s_1/R_B	a/R_B	b/R_B	r_b/R_B
	1	0.707	0	-	-	0.824	0.809
	2	0.707	0.2	1.005	0.495	0.857	0.852
	3	0.707	0.4	0.885	0.596	1.005	0.853
	4	0.417	0	-	-	0.656	0.798
	5	0.417	0.2	0.887	0.350	0.779	0.821
	6	0.417	0.4	0.727	0.492	0.929	0.840
	7	0	0	-	-	0.632	0.748
	8	0	0.2	0.800	0.200	0.672	0.800
	9	0	0.4	0.600	0.400	0.836	0.838

Figure 1.- Model geometry and dimensions.

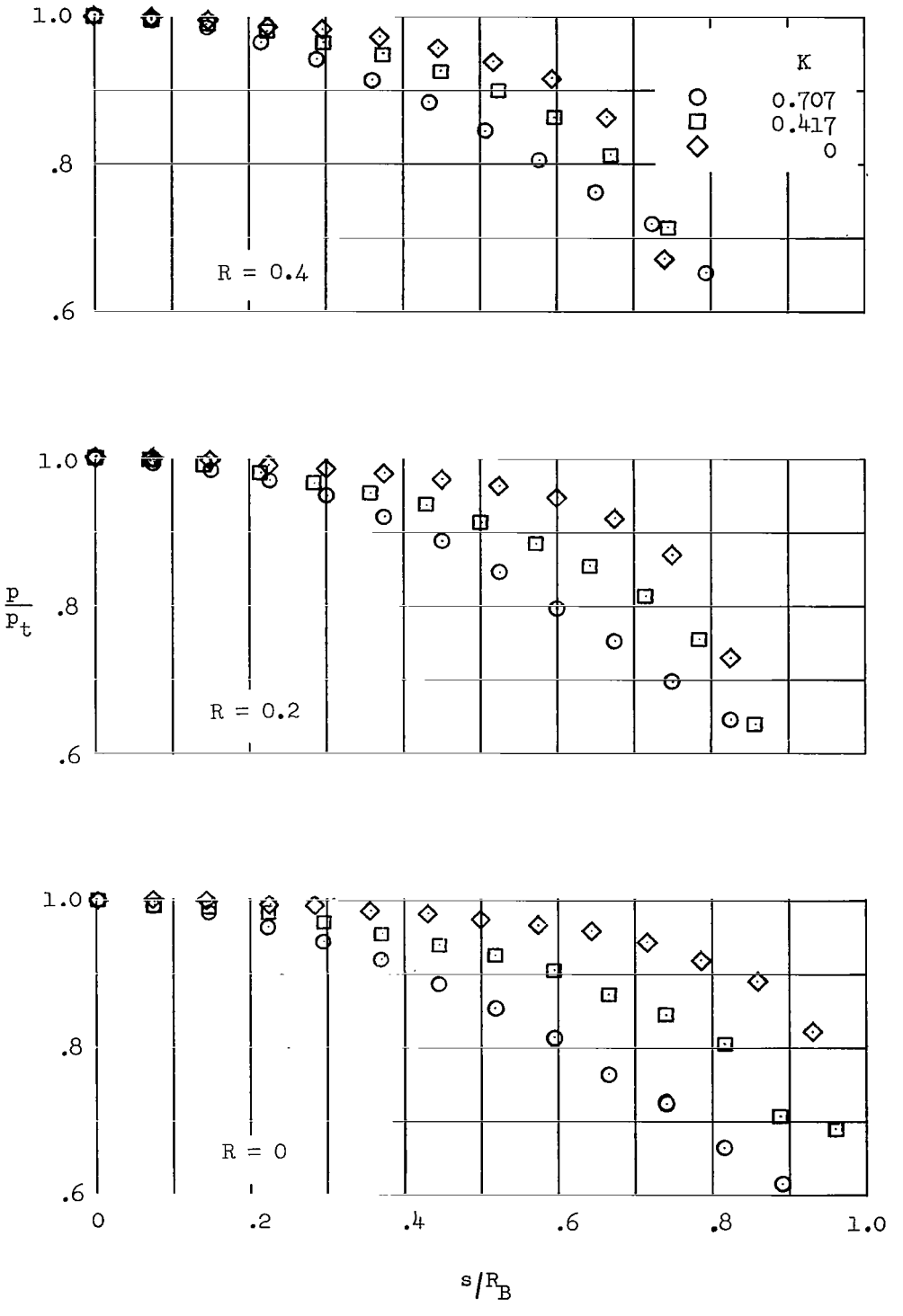

Figure 2.- Effects of model geometry on local pressures. $\alpha = 0^0$.

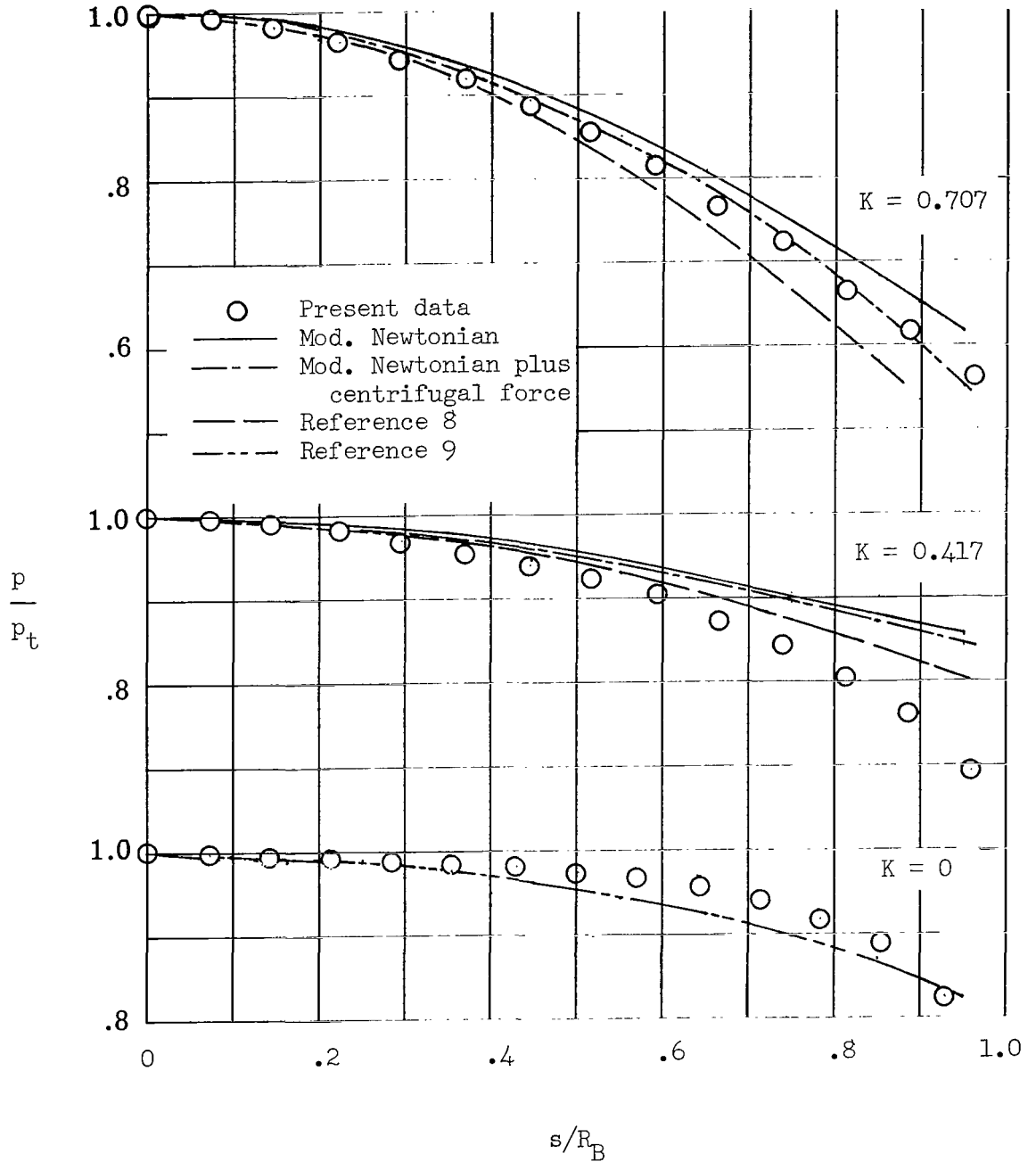

Figure 3.- Comparison of experimental and theoretical pressure distributions. $\alpha = 0^{o}$; R = 0.

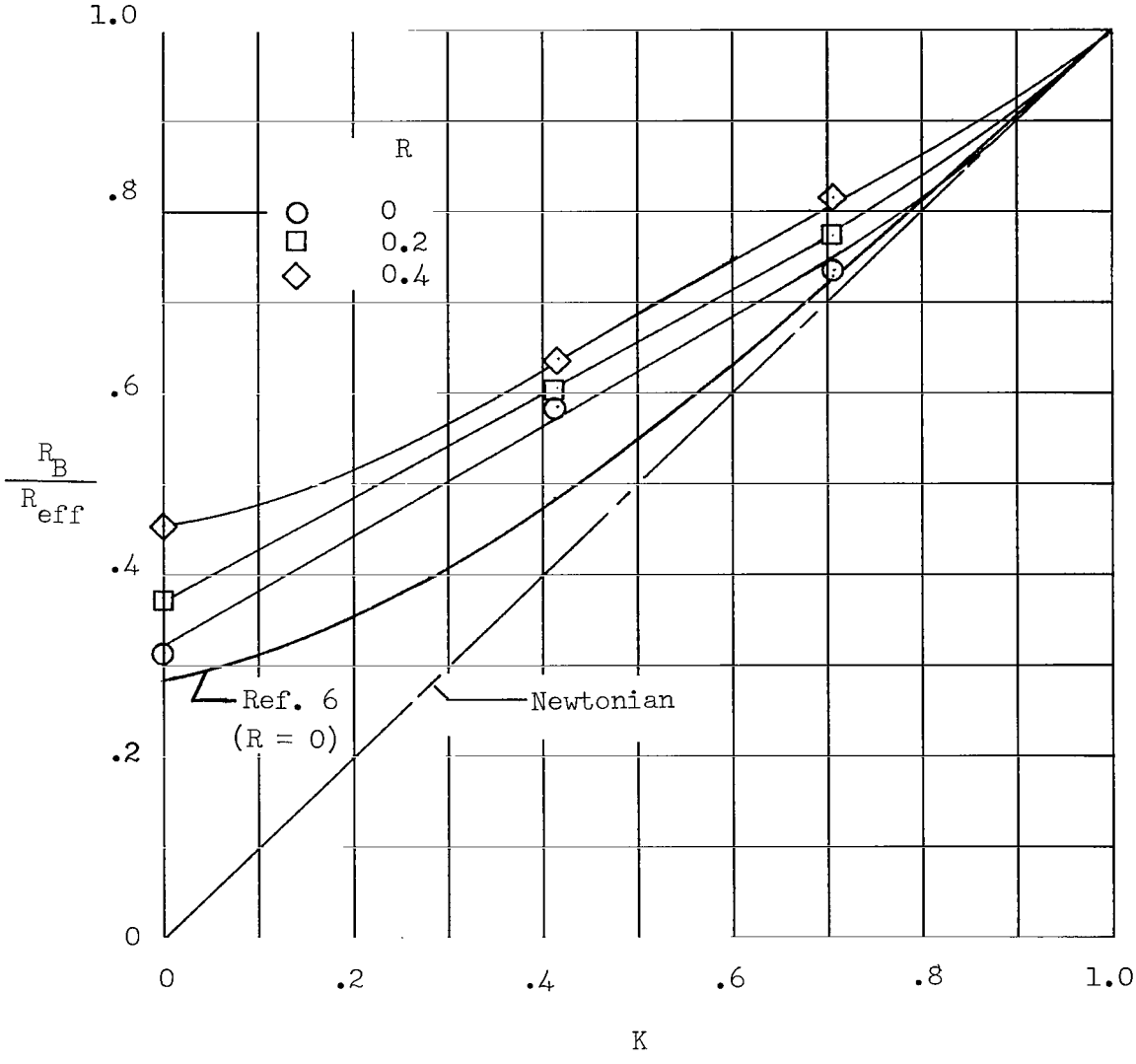

(a) Effect of nose radius.

Figure 4.- Effect of body geometry on the effective nose radius. $\alpha = 0^{o}$.

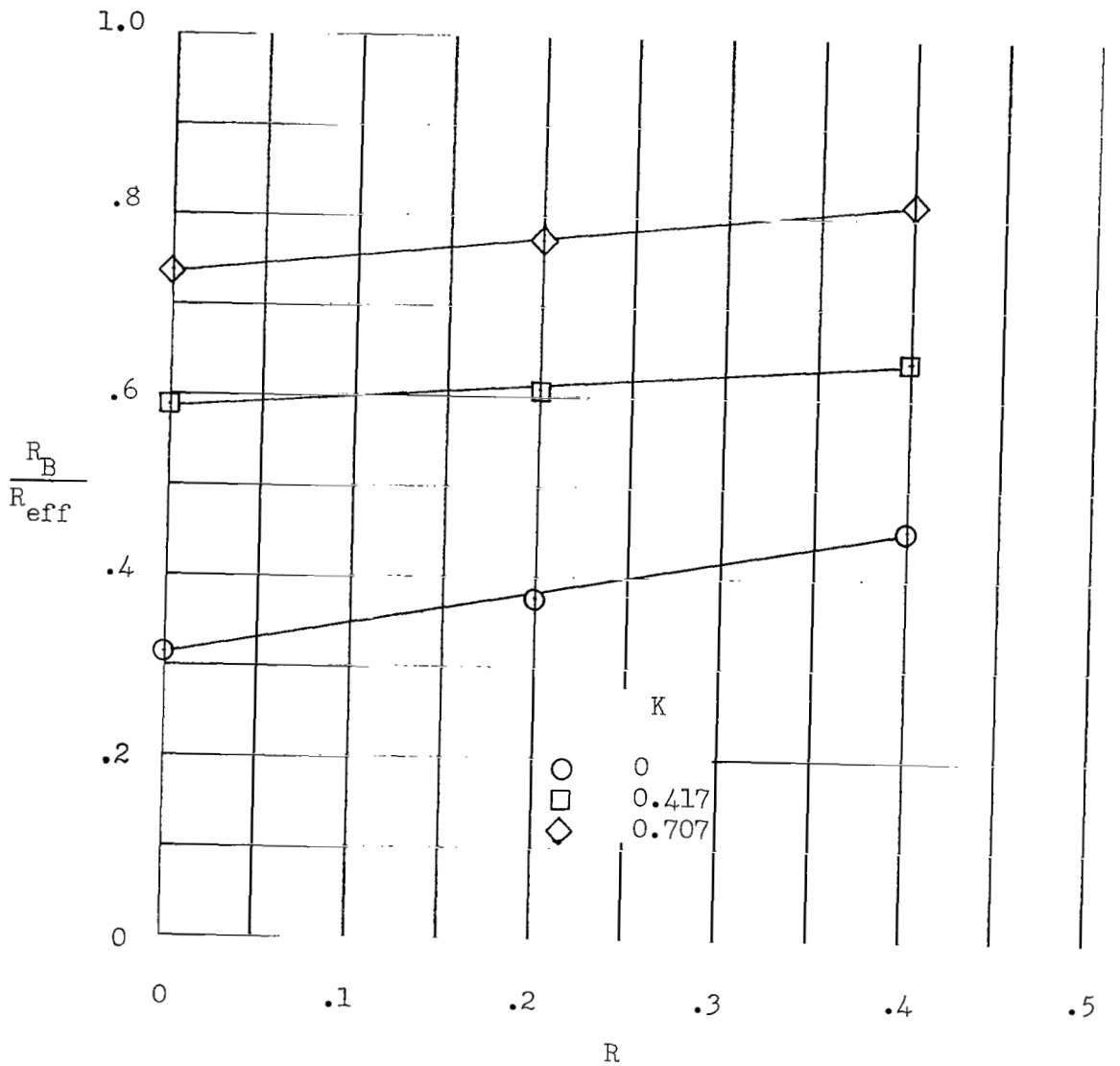

(b) Effect of corner radius.

Figure 4.- Concluded.

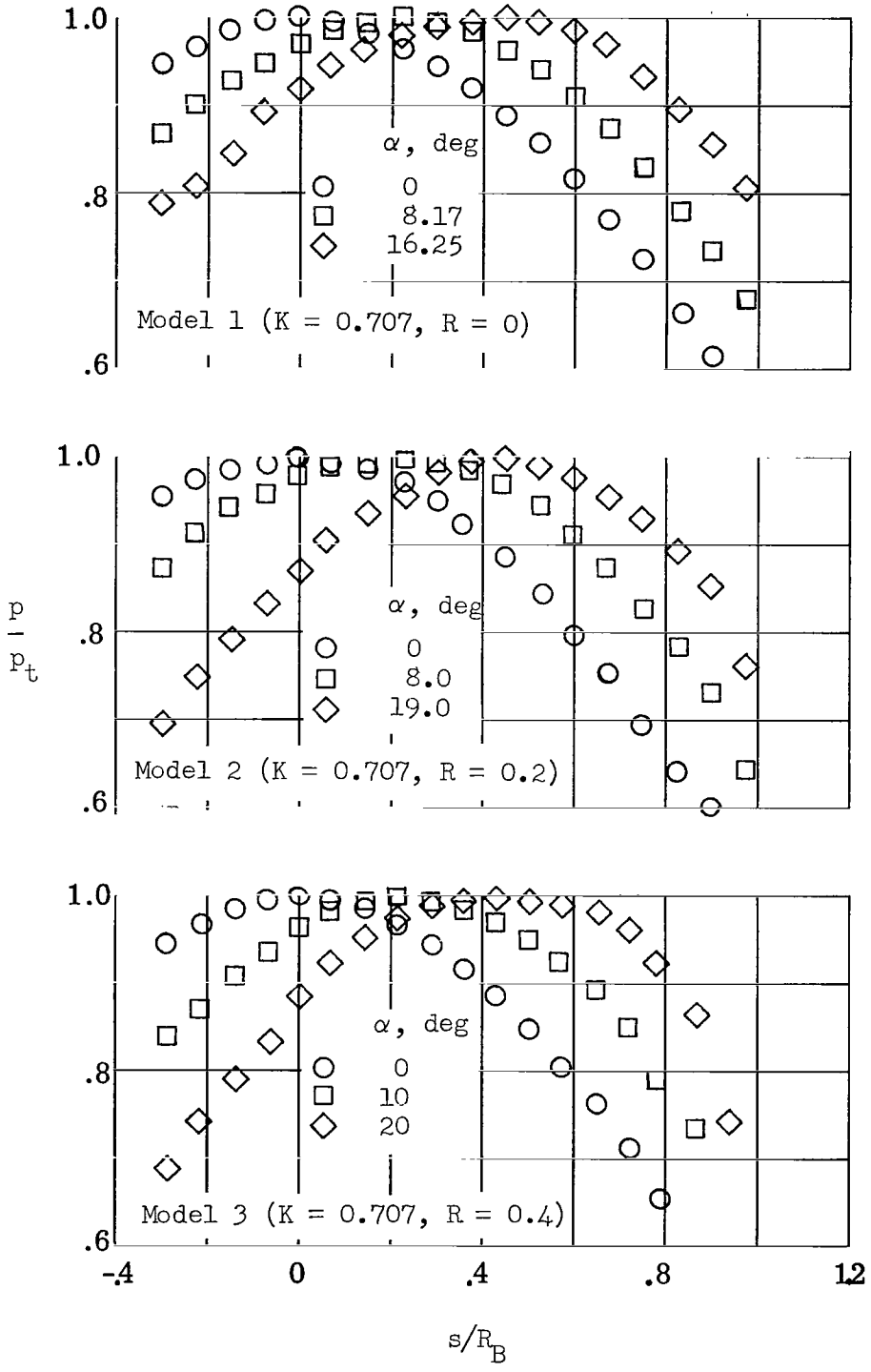

Figure 5.- Local pressure distributions at angles of attack.

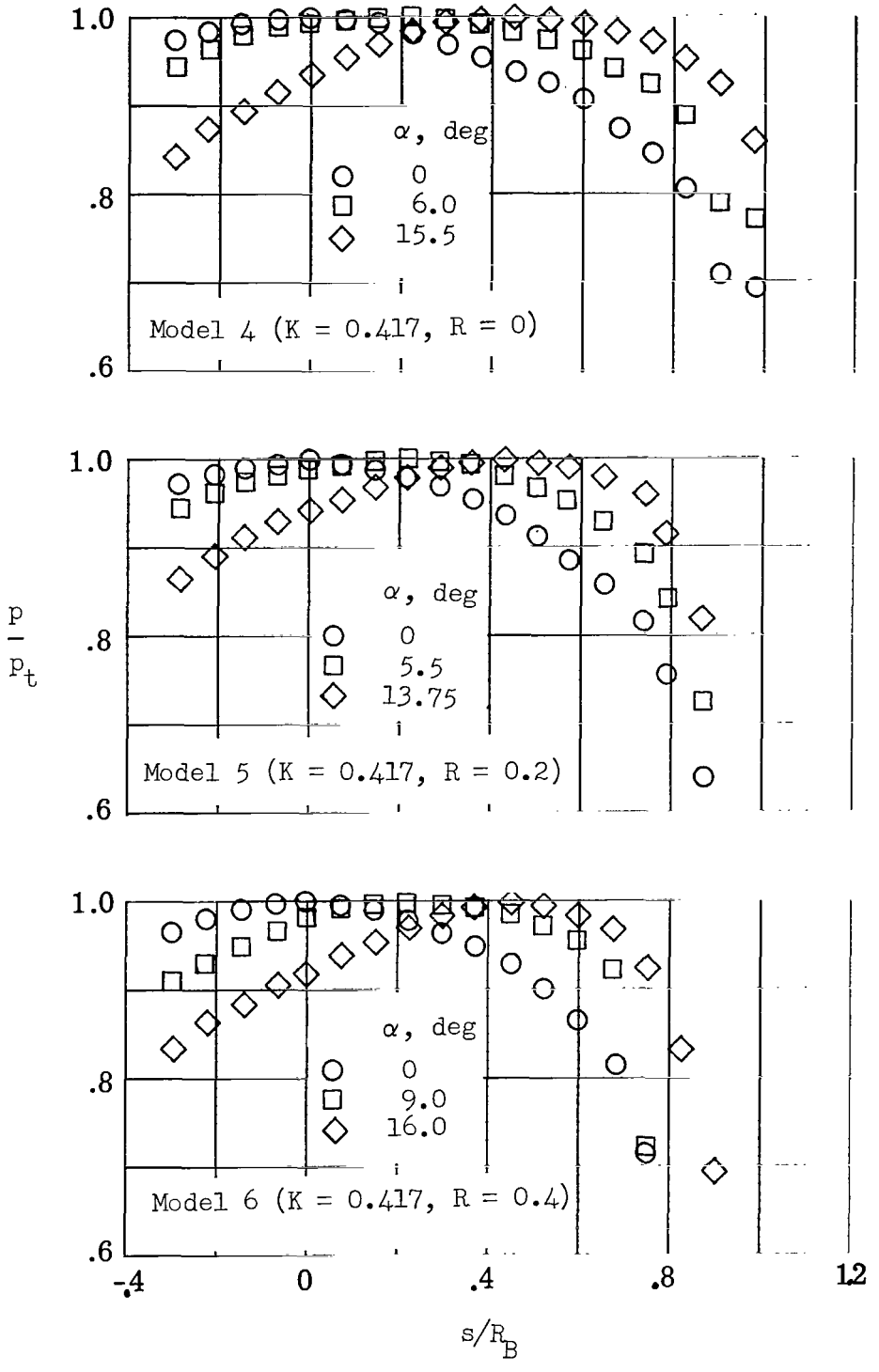

Figure 5.- Continued.

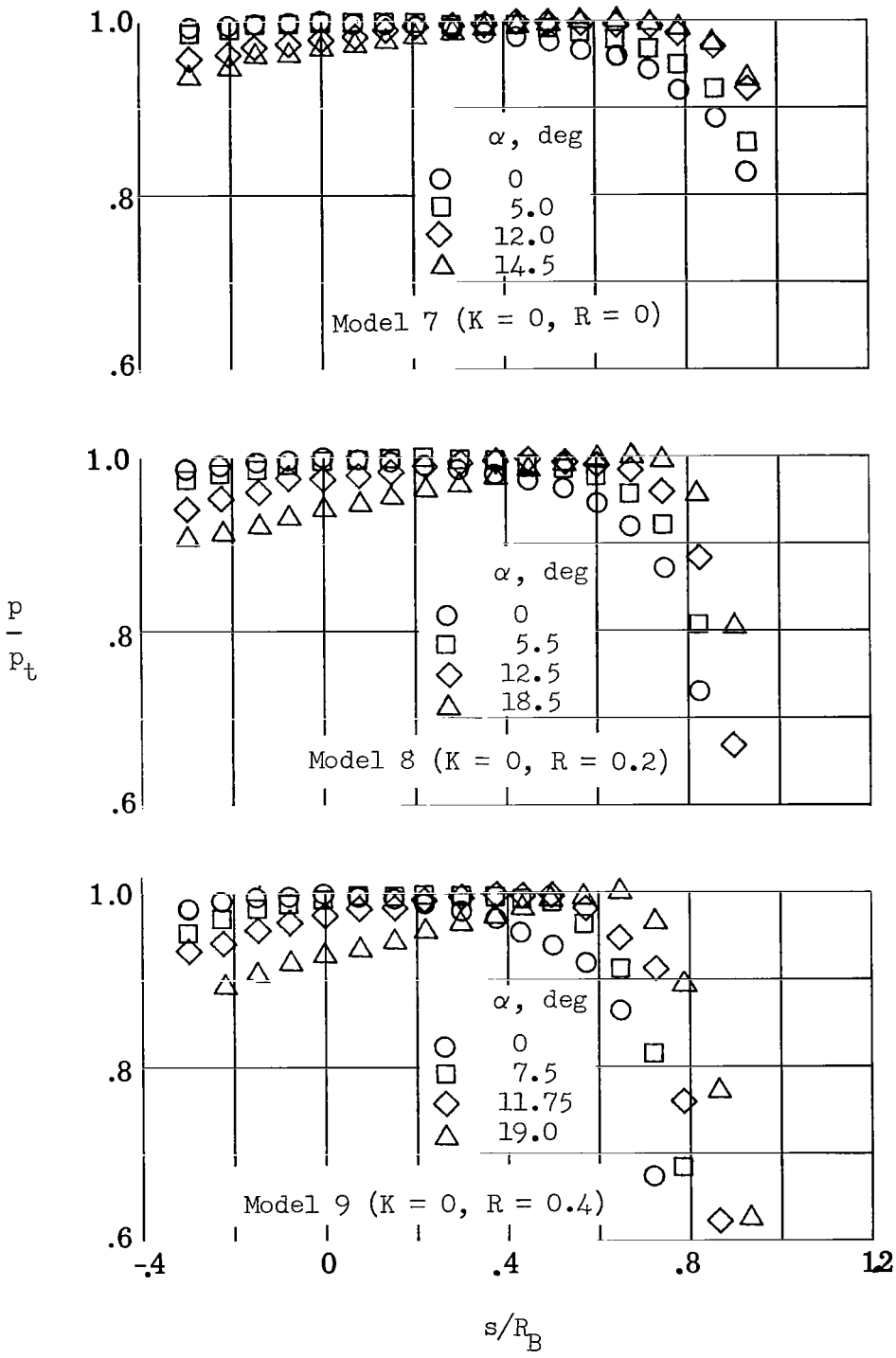

Figure 5.- Concluded.

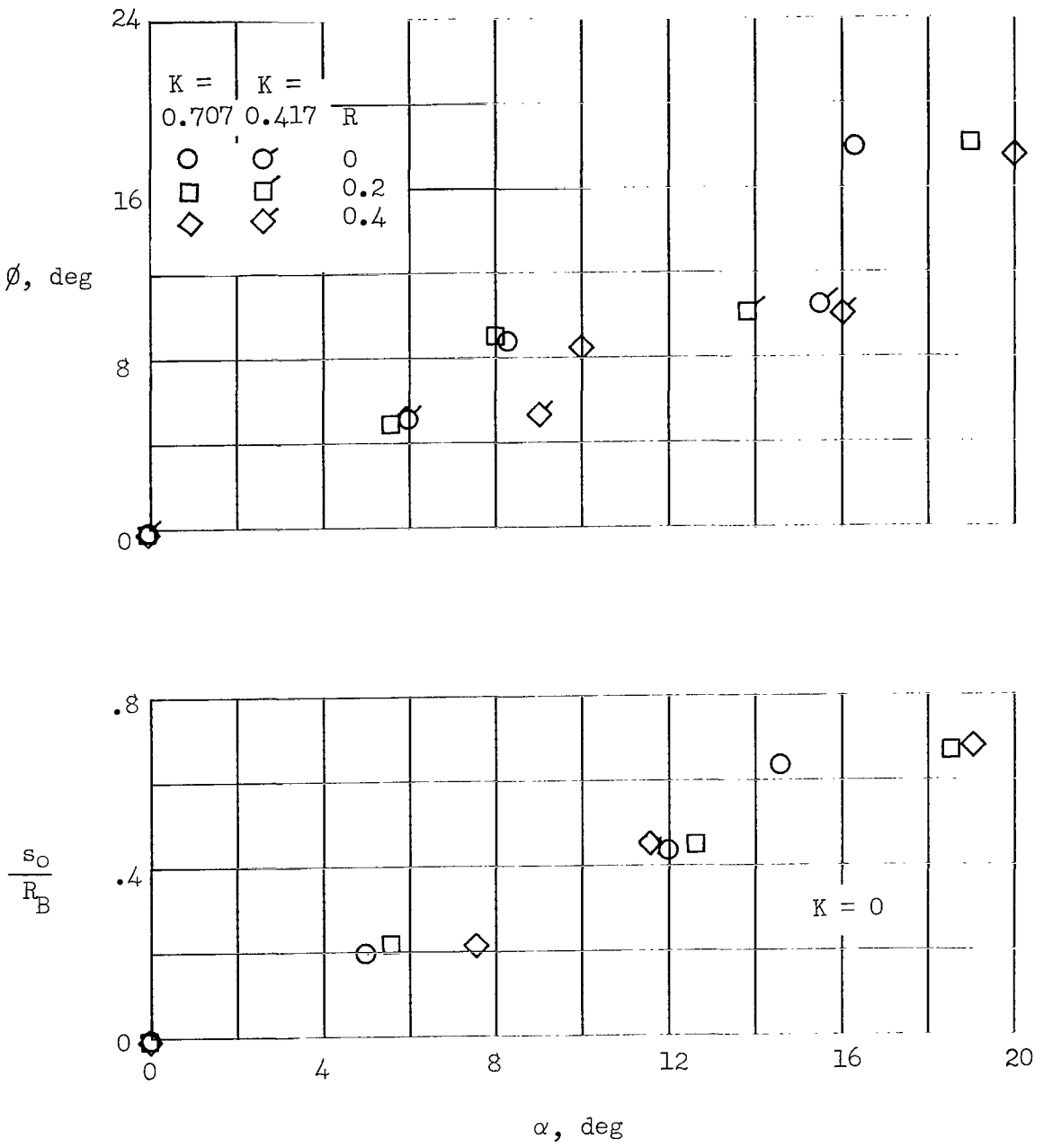

Figure 6.- Location of stagnation point at angles of attack.

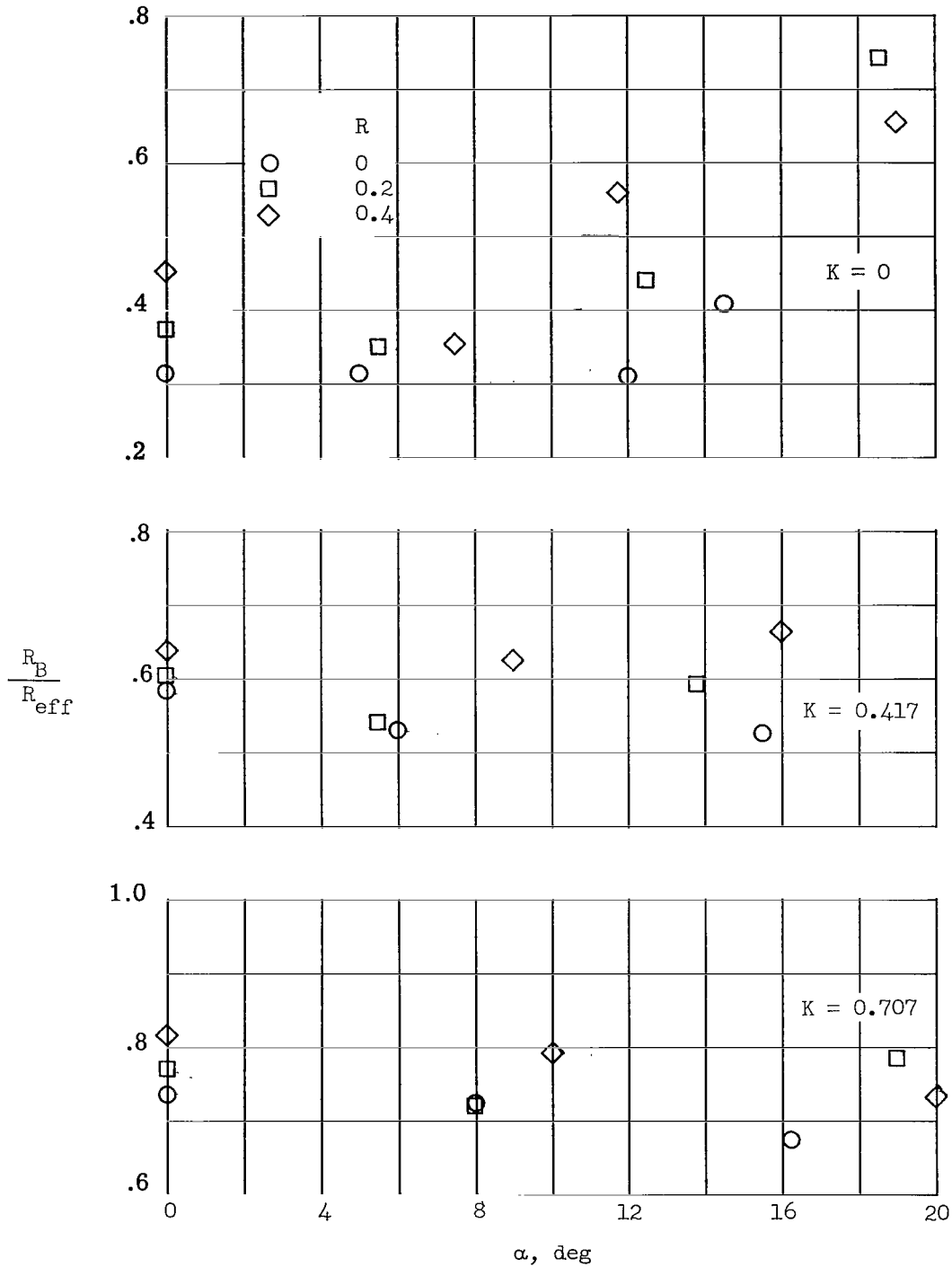

Figure 7.- Effect of angle of attack on the effective nose radius.

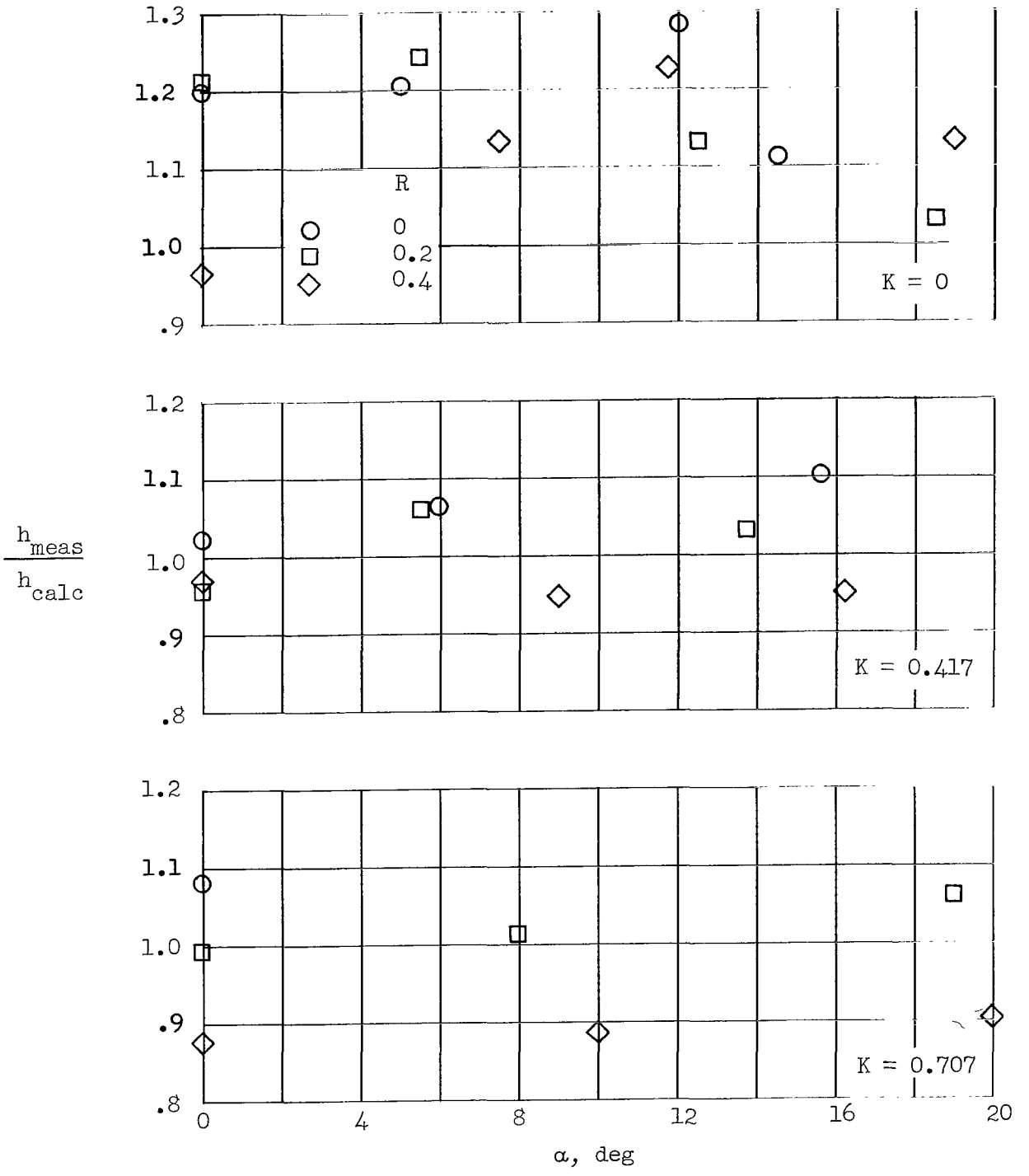

Figure 8.- Effect of angle of attack on heat transfer.

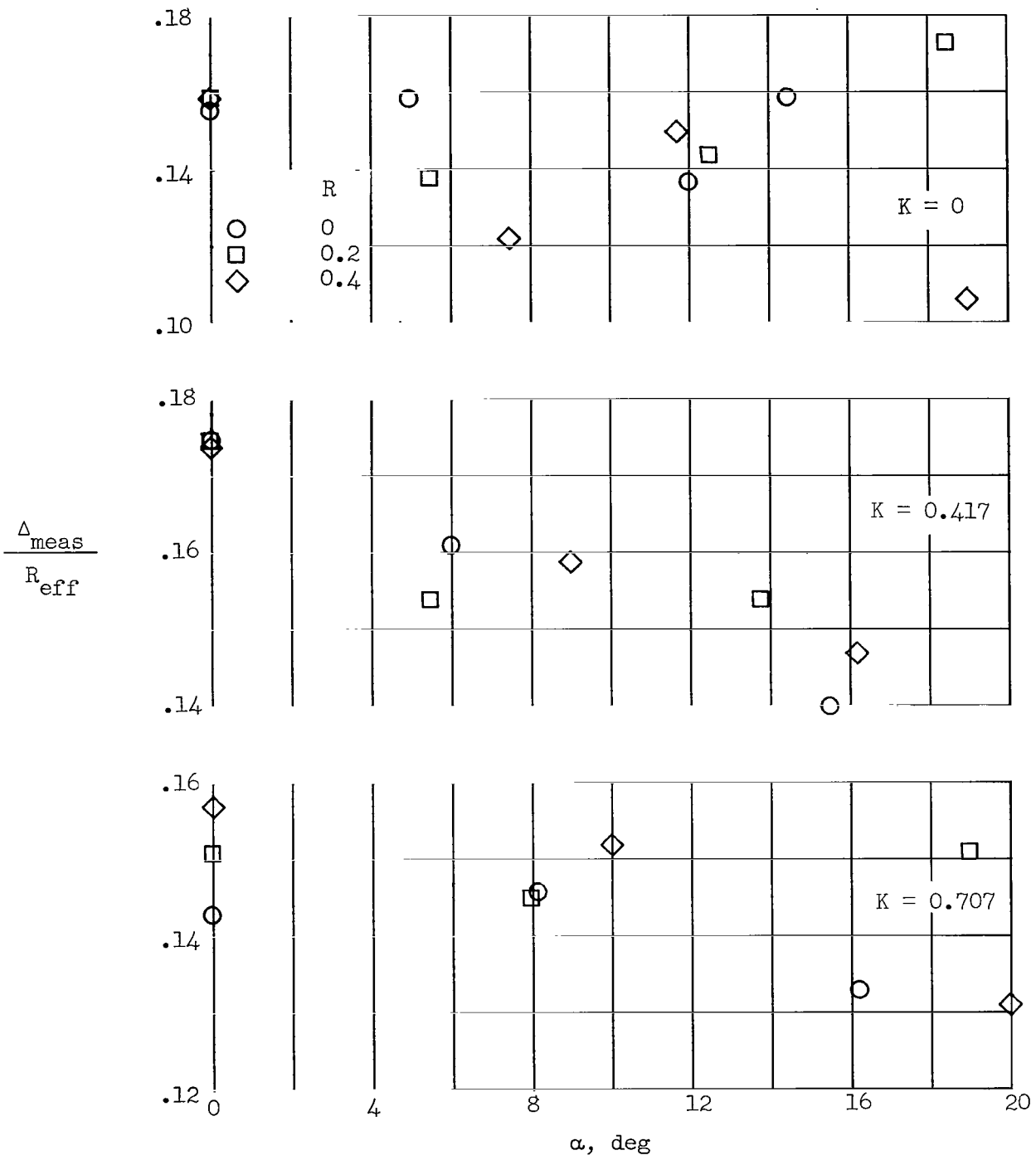

Figure 9.- Effect of angle of attack on shock detachment distance.

NATIONAL AERONAUTICS AND SPACE ADMINISTRATION
WASHINGTON, D.C. 20546

OFFICIAL BUSINESS

FIRST CLASS MAIL

POSTAGE AND FEES PAID
NATIONAL AERONAUTICS AND
SPACE ADMINISTRATION

POSTMASTER: If Undeliverable (Section 158 Postal Manual) Do Not Return

"The aeronautical and space activities of the United States shall be conducted so as to contribute . . . to the expansion of human knowledge of phenomena in the atmosphere and space. The Administration shall provide for the widest practicable and appropriate dissemination of information concerning its activities and the results thereof."

—NATIONAL AERONAUTICS AND SPACE ACT OF 1958

NASA SCIENTIFIC AND TECHNICAL PUBLICATIONS

TECHNICAL REPORTS: Scientific and technical information considered important, complete, and a lasting contribution to existing knowledge.

TECHNICAL NOTES: Information less broad in scope but nevertheless of importance as a contribution to existing knowledge.

TECHNICAL MEMORANDUMS: Information receiving limited distribution because of preliminary data, security classification, or other reasons.

CONTRACTOR REPORTS: Scientific and technical information generated under a NASA contract or grant and considered an important contribution to existing knowledge.

TECHNICAL TRANSLATIONS: Information published in a foreign language considered to merit NASA distribution in English.

SPECIAL PUBLICATIONS: Information derived from or of value to NASA activities. Publications include conference proceedings, monographs, data compilations, handbooks, sourcebooks, and special bibliographies.

TECHNOLOGY UTILIZATION PUBLICATIONS: Information on technology used by NASA that may be of particular interest in commercial and other non-aerospace applications. Publications include Tech Briefs, Technology Utilization Reports and Notes, and Technology Surveys.

Details on the availability of these publications may be obtained from:

SCIENTIFIC AND TECHNICAL INFORMATION DIVISION

NATIONAL AERONAUTICS AND SPACE ADMINISTRATION

Washington, D.C. 20546